

Voronoi cell volume distribution and configurational entropy of hard-spheres

V. Senthil Kumar and V. Kumaran^{a)}

Department of Chemical Engineering, Indian Institute of Science, Bangalore 560 012, India

(Received 7 March 2005; accepted 8 July 2005; published online 16 September 2005)

The Voronoi cell volume distributions for hard-disk and hard-sphere fluids have been studied. The distribution of the Voronoi free volume v_f , which is the difference between the actual cell volume and the minimal cell volume at close packing, is well described by a two-parameter (2Γ) or a three-parameter (3Γ) gamma distribution. The free parameter m in both the 2Γ and 3Γ models is identified as the “regularity factor.” The regularity factor is the ratio of the square of the mean and the variance of the free volume distribution, and it increases as the cell volume distribution becomes narrower. For the thermodynamic structures, the regularity factor increases with increasing density and it increases sharply across the freezing transition, in response to the onset of order. The regularity factor also distinguishes between the dense thermodynamic structures and the dense random or quenched structures. The maximum information entropy (max-ent) formalism, when applied to the gamma distributions, shows that structures of maximum information entropy have an exponential distribution of v_f . Simulations carried out using a swelling algorithm indicate that the dense random-packed states approach the distribution predicted by the max-ent formalism, though the limiting case could not be realized in simulations due to the structural inhomogeneities introduced by the dense random-packing algorithm. Using the gamma representations of the cell volume distribution, we check the numerical validity of the Cohen-Grest expression [M. H. Cohen and G. S. Grest, *Phys. Rev. B* **20**, 1077 (1979)] for the cellular (free volume) entropy, which is a part of the configurational entropy. The expression is exact for the hard-rod system, and a correction factor equal to the dimension of the system, D , is found necessary for the hard-disk and hard-sphere systems. Thus, for the hard-disk and hard-sphere systems, the present analysis establishes a relationship between the precisely defined Voronoi free volume (information) entropy and the thermodynamic entropy. This analysis also shows that the max-ent formalism, when applied to the free volume entropy, predicts an exponential distribution which is approached by disordered states generated by a swelling algorithm in the dense random-packing limit. © 2005 American Institute of Physics. [DOI: 10.1063/1.2011390]

I. INTRODUCTION

The Voronoi polyhedron of a point nucleus in space is the smallest polyhedron formed by the perpendicularly bisecting planes between a given nucleus and all the other nuclei.¹ The Voronoi tessellation divides a region into space-filling, nonoverlapping convex polyhedra. The salient properties of Voronoi tessellation are the following:

- Any point inside a Voronoi cell is closer to its nucleus than to any other nuclei (Fig. 1). These cells are space filling and hence give a precise definition of local volume.²
- It gives a definition of geometric neighbors. The nuclei sharing a common Voronoi surface are geometric neighbors. Points on the shared surface are equidistant to the corresponding pair of nuclei. Hence geometric neighbors are competing centers in a growth scenario.
- The Voronoi cells of hard-spheres are irregular at lower packing fractions but become regular as the regular

close packing is approached. Thus, they are useful in characterizing all structures, from random to regular.

These properties qualify Voronoi tessellation as an important tool in the structural analysis of random media such

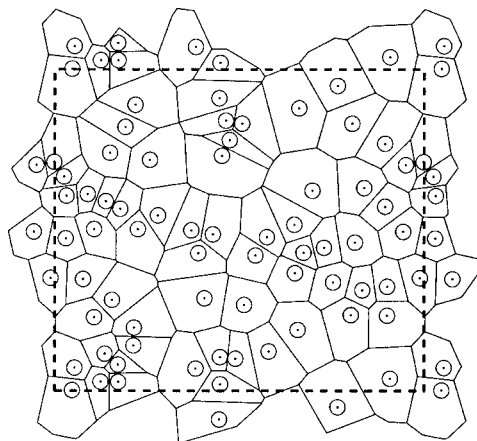


FIG. 1. The Voronoi tessellation of a hard-disk configuration, with periodic boundary conditions. The central box shown in dashed lines.

^{a)}Electronic mail: kumaran@chemeng.iisc.ernet.in

as glass, packings, foams, cellular solids, proteins, etc.³⁻⁵ Voronoi tessellation occurs naturally in growth processes such as crystallization and plant cell growth.⁶ It is used (and even rediscovered under different names) in various fields like meteorology, geology, ecology, metallography, archeology, etc. The statistical distributions of many Voronoi cell properties are reported (see Zhu *et al.*,⁷ Oger *et al.*,⁸ and references therein). In this work, we focus on the cell volume distributions and their utility in computing the configurational entropy of hard-sphere systems.

In this work we define the *Voronoi free volume* of any hard particle as the difference between its Voronoi volume and the minimal cell volume occurring at a regular close packing. Since there are varied notions of free volume, we list below the Bondi⁹ classification of free volumes.

- (1) Empty volume = $V - V_w$, where V is the observed molar volume of the fluid and V_w is the van der Waal's volume of the fluid. V_w is the volume occupied by a molecule, which is impenetrable for the other molecules, at a given temperature. It is the soft potential generalization of the exclusion sphere concept used in the hard-sphere systems. It is widely used as the molecular steric descriptor to correlate physicochemical properties¹⁰ and biological activity.¹¹ The free volume used in the fluctuating cell theory^{12,13} is an empty volume.
- (2) (Thermal) Expansion volume = $V - V_0$, where V_0 is the molar volume of the substance in its crystalline state at absolute zero temperature. The Voronoi free volume used in this work is the microscopic version of expansion volume. The free volume used in the Doolittle fluidity equation¹⁴ is an expansion volume, but with V_0 in a hypothetical state without a phase change. This is the most widely used free volume in the glassy polymer literature.¹⁵ However, the other two free volumes are also used.^{16,17} There are a few experimental measures of free volume which do not clearly fit into this classification.¹⁸
- (3) Fluctuation volume = $N_A v_\phi$, where v_ϕ is the volume swept by the center of gravity of the molecule due to thermal motion and N_A is Avogadro's constant. This is the notion of free volume used in the lattice or regular cell theories.¹⁹

Section II analyzes the two-parameter (2Γ) and the three-parameter (3Γ) gamma distributions used to represent the free volume distributions of hard-disk and hard-sphere systems. After imposing the specific-volume constraint, the 2Γ and 3Γ distributions have, respectively, one and two free parameters. The free parameter m in both the 2Γ and 3Γ models is identified as a structural order parameter called the regularity factor. In Sec. III using a maximum information entropy (max-ent) formalism, based on the notion that for an ordered state all the cell volumes are identical, we predict that the free volume distribution is exponential for an *ideal* dense random-packed state. In Sec. IV we present the simulation results for the thermodynamic and random structures of hard-disk and hard-sphere systems. For the thermodynamic structures, the regularity factor increases with increasing density and it increases sharply across the freezing tran-

sition, in response to the onset of order. The regularity factor also distinguishes between the dense thermodynamic structures and the dense random structures. The max-ent prediction for the dense random packing seems to be approached but not exactly reached due to the structural inhomogeneities introduced by the dense random-packing algorithm used. In Sec. V, using the 2Γ model, we check the Cohen-Grest ansatz for configurational entropy and find that ansatz is exact for the hard-rod system, and a factor equal to the dimension of the system is found missing in the original ansatz for the hard-disk and hard-sphere systems. This first-order homogeneity of the entropy in the dimension of the system, D , is anticipated if the number of states of an independent particle increases with D as 2^D .

II. CELL VOLUME DISTRIBUTION

The Voronoi cells of hard-rods, hard-disks, and hard-spheres are segments, polygons, and polyhedra respectively, and *volume* correspondingly means, length, area, and solid volume. Let v be any individual Voronoi cell volume and $f(v)$ its distribution. Let v_p be the volume of the hard particle and \bar{v} the average Voronoi cell volume (identical to a specific volume, since the Voronoi cells are space filling). Then, the packing fraction ν is given by $\nu = v_p / \bar{v}$. At low ν the Voronoi cells are irregular, and as ν increases the cells become more regular. At the regular close packing, all the cells are identical, and the distribution is reduced to a Dirac delta distribution. Let v_c be the Voronoi cell volume at the regular close packing. For hard-rods v_c is the length of the hard-rod, for hard-disks it is the regular hexagon circumscribing the hard-disk, and for hard-spheres it is the rhombic dodecahedron circumscribing the hard-sphere (corresponding to face-centered-cubic (fcc) structure). The packing fraction at the regular close packing is $\nu_c = v_p / v_c$, and the normalized packing fraction is $y = \nu / \nu_c$.

Other packing fractions of physical relevance are

- the freezing (ν_F) and melting (ν_M) packing fractions,
- the loose random packing (ν_{LRP}) defined²⁰ as the lowest-density isotropic packing that can support an infinitesimal external load at the limit of acceleration due to gravity tending to zero, and
- the dense random packing (ν_{DRP}) which is the highest-density homogeneous isotropic packing.

All these salient packing fractions and the entropy change per particle due to the freezing transition are listed in Table I. There is no freezing transition for a hard-rod system. Also there are no random structures for hard-rods since the regular close packing is the only load-bearing structure.

It is customary to fit the cell volume distribution data for random points (Poisson-Voronoi tessellation) to a 2Γ or a 3Γ distribution given in Table II (read with $v_j = v$). The subscript "0" is used to indicate the low density or the Poisson limit. Using the specific-volume criteria we get,

TABLE I. Salient properties of hard-rods, hard-disks, and hard-spheres.

	Hard-rod	Hard-disk	Hard-sphere
σ	Length	Diameter	Diameter
Volume of the particle, v_p	σ	$\frac{\pi}{4}\sigma^2$	$\frac{\pi}{6}\sigma^3$
Cell volume at regular close packing v_c	σ	$\frac{\sqrt{3}}{2}\sigma^2$	$\frac{1}{\sqrt{2}}\sigma^3$
Freezing packing fraction, ν_F	...	$\approx 0.691^a$	$\approx 0.494^b$
Entropy change per particle on freezing $\Delta S_F/k_B$...	$\approx 0.36^a$	$\approx 1.16^b$
Melting packing fraction, ν_M	...	$\approx 0.716^a$	$\approx 0.545^b$
Loose random packing, ν_{LRP}	...	0.772 ± 0.002^c	0.555 ± 0.005^d
Dense random packing, ν_{DRP}	...	0.82 ± 0.02^e	0.64 ± 0.02^e
Regular close packing, ν_c	1	$\frac{\pi}{2\sqrt{3}}$	$\frac{\pi}{3\sqrt{2}}$

^aFrom Alder and Wainwright (Ref. 48).^bFrom Hoover and Ree (Ref. 49).^cFrom Hinrichsen *et al.* (Ref. 24).^dFrom Onoda and Liniger (Ref. 20).^eFrom Berryman (Ref. 50).

$$\alpha_0 = \begin{cases} \frac{m_0}{\bar{v}}, & 2\Gamma \text{ model;} \\ \left[\frac{\Gamma((m_0 + \delta_0)/\delta_0^2)}{\Gamma(m_0/\delta_0^2)\bar{v}} \right] \delta_0, & 3\Gamma \text{ model.} \end{cases} \quad (1)$$

The reported best-fit values of the free parameters m_0 for 2Γ and m_0, δ_0 for 3Γ models) are given in Table III. Note that only the one-dimensional (1D) results are exact. Heuristic arguments in Weaire *et al.*²¹ show that the cell area distributions for a two-dimensional (2D) Poisson tessellation can be approximated by a 2Γ distribution.

For a hard-core tessellation, some studies like Hermann *et al.*²² and Gotoh²³ fit the 2Γ model for the cell volume, i.e., $v_f = v$ in Table II. The volume of any Voronoi cell will be greater or equal to v_c ; hence the above fit gives an unphysical nonzero value for $\int_0^{v_c} f(v)dv$. Alternatively, for a hard-core tessellation, the 2Γ or 3Γ models can be fitted with $v_f = v - v_c$ in Table II, where v_f is the Voronoi free volume. In

Sec. V, we show that this definition of free volume gets the thermodynamic singularity correctly at the regular close packing. In Hinrichsen *et al.*²⁴ the Voronoi free volume fit is used in the study of loose random packing. Note that this fit accommodates the gamma representation at the Poisson limit, where $\sigma=0$ and hence $v_c=0$ and $v_f=v$. Now, we show that the Voronoi free volume arises spontaneously in the hard-rod system. For the hard-rod system the nearest-neighbor distance distribution function $f(x)$ is exactly known (see Fisher²⁵),

$$f(x) = \begin{cases} 0 & \text{if } x < \sigma; \\ \frac{1}{(\bar{v} - \sigma)} \exp\left[-\frac{(x - \sigma)}{(\bar{v} - \sigma)}\right] & \text{if } x \geq \sigma. \end{cases} \quad (2)$$

In Fig. 2, let x_i be the distance between the centers of the hard-rods P_{i-1} and P_i and let x_{if} be the free distance between their tips, then $x_{if} = x_i - \sigma$. Then, the Voronoi segment for P_i

TABLE II. Properties of two-parameter (2Γ) and three-parameter (3Γ) gamma distributions.

Property	2Γ distribution	3Γ distribution ^{a, b}
Distribution, $f(v_f)$	$\frac{\alpha^m}{\Gamma(m)} v_f^{m-1} e^{-\alpha v_f}$	$\frac{\delta \alpha^{(m/\delta^2)}}{\Gamma(m/\delta^2)} v_f^{(m/\delta^2)-1} e^{-\alpha v_f^\delta}$
$0 \leq v_f < \infty$	$m, \alpha > 0$	$m, \delta, \alpha > 0$
Mean = \bar{v}_f	$\frac{m}{\alpha}$	$\frac{\Gamma((m+\delta)/\delta^2)}{\Gamma(m/\delta^2)\alpha^{1/\delta}}$
Variance = $\sigma^2(v_f) = \bar{v}_f^2 - (\bar{v}_f)^2$	$\frac{m(m+1)}{\alpha^2} - \left(\frac{m}{\alpha}\right)^2 = \frac{m}{\alpha^2}$	$\frac{\Gamma((m+2\delta)/\delta^2)}{\Gamma(m/\delta^2)\alpha^{2/\delta}} - \left[\frac{\Gamma((m+\delta)/\delta^2)}{\Gamma(m/\delta^2)\alpha^{1/\delta}}\right]^2$
Standard deviation = $\frac{\sigma(v_f)}{\text{Mean}} = \frac{\sigma(v_f)}{v_f}$	$\frac{1}{\sqrt{m}}$	$\left[\frac{\Gamma(m/\delta^2)\Gamma((m+2\delta)/\delta^2)}{[\Gamma((m+\delta)/\delta^2)]^2} - 1\right]^{1/2}$

^aWith $\delta=1$ and using $\Gamma(m+1)=m\Gamma(m)$, the 3Γ results are reduced to the 2Γ results.^bGenerally the 3Γ model is written as $f(v_f) = (\delta \alpha^{(m/\delta)}/\Gamma(m/\delta)) v_f^{(m/\delta)-1} e^{-\alpha v_f^\delta}$ [see, for example, Tanemura (Ref. 51)]. Using $\tilde{m}=m/\delta$ we get the above form. This form has the advantage that m is the regularity factor in both the 2Γ and 3Γ models.

TABLE III. Parameters of 2Γ and 3Γ models for the cell volume distribution of a D -dimensional Poisson tessellation.

D	m_0	δ_0^a	Reference
1	2	1	Exact result, Kiang (Ref. 52)
2	3.5	1	Kiang's revised value, as in Ref. 21
2	3.61	1	Weaire <i>et al.</i> (Ref. 21)
2	3.57	1	DiCenzo and Wertheim (Ref. 53)
2	3.57782	1	Current work, Fig. 3
2	3.5700	1.0787	Hinde and Miles (Ref. 54)
2	3.57371	1.07805	Tanemura (Ref. 51)
2	3.63454	1.09577	Current work, Fig. 3
3	6	1	Kiang (Ref. 52)
3	5.56	1	Andrade and Fortes (Ref. 55)
3	5.56219	1	Current work, Fig. 13
3	5.59434	1.16391	Tanemura (Ref. 51)
3	5.68147	1.19361	Current work, Fig. 13
4	8.41715	1.29553	Tanemura (Ref. 51)

^a $\delta_0=1$ implies a 2Γ model and $\delta_0 \neq 1$ a 3Γ model.

is given by $v=(x_1+x_2)/2=(x_{1f}+x_{2f})/2+\sigma$. Noting that in 1D $v_c=\sigma$, we have $v_f=v-v_c=(x_{1f}+x_{2f})/2$. Say $l=2v_f=x_{1f}+x_{2f}$. Here, x_{1f} and x_{2f} are independent, since the free distances x_{if} do not percolate. Then the cumulative distribution function of l is

$$F(l) = \int_0^l dx_{2f} \int_0^{l-x_{2f}} dx_{1f} f(x_{1f}) f(x_{2f}). \quad (3)$$

Using $f(x_f)=a \exp(-ax_f)$ with $a=1/(\bar{v}-\sigma)$ gives

$$\begin{aligned} F(l) &= \int_0^1 a e^{-ax_{2f}} dx_{2f} \int_0^{l-x_{2f}} a e^{-ax_{1f}} dx_{1f} \\ &= 1 - \exp(-al) - al \exp(-al). \end{aligned}$$

Then, the probability distribution function for l is given by

$$f(l) = \frac{dF(l)}{dl} = a^2 l \exp(-al).$$

Using $l=2v_f$ in $f(v_f)dv_f=f(l)dl$ we get

$$f(v_f) = (2a)^2 v_f \exp(-2av_f).$$

With $\alpha=2a$ and $m=2$, it can be written as

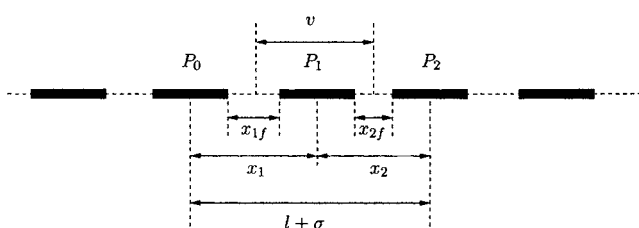


FIG. 2. Hard-rods along a line. Hard-rod length is σ .

$$f(v_f) = \frac{\alpha^m}{\Gamma(m)} v_f^{(m-1)} \exp(-\alpha v_f).$$

Thus for the hard-rod system at any v , the Voronoi free volume follows a 2Γ distribution with $m=2$. This suggests fitting a 2Γ or its generalization the 3Γ distribution (Table II) for $f(v_f)$ in hard-disk and hard-sphere systems. The free parameter in the 2Γ model is m , and the free parameters in the 3Γ model are m and δ . α is computed using the specific volume criteria as

$$\alpha = \begin{cases} \frac{m}{\bar{v}(1-y)}, & 2\Gamma \text{ model;} \\ \left[\frac{\Gamma((m+\delta)/\delta^2)}{\Gamma(m/\delta^2)\bar{v}(1-y)} \right]^\delta, & 3\Gamma \text{ model.} \end{cases} \quad (4)$$

Here, we have used $\bar{v}_f = \bar{v} - v_c = \bar{v}(1-y)$. Note that at $y=1$, α diverges and the variance becomes zero, so that the gamma distribution is reduced to the Dirac delta distribution. The simulation results in Sec. IV show that m does not diverge at the regular close-packed limit.

In the 2Γ model, the ratio of the standard deviation and mean is $1/\sqrt{m}$ (Table II). This shows that as m increases, the spread of the distribution about the mean decreases; i.e., the cells become more regular. Hence m is called regularity factor in Gotoh²³ (This work, however, used the 2Γ model for $f(v)$ rather than $f(v_f)$, as mentioned earlier). As y increases, the thermodynamic structures become more regular, and hence m increases. At the freezing transition, due to the onset of order, there is a sharp increase in m . Thus m is a useful scalar parameter characterizing the hard-disk and hard-sphere structures. In the hard-rod system, since $m=2$ for any v , the ratio of the standard deviation to the mean is constant, a hallmark of the absence of the fluid-solid transition in this system.

A physical interpretation for the parameter m in the 3Γ model can be obtained by using the $n \rightarrow \infty$ asymptotic expansion from Spanier and Oldham,²⁶

$$\begin{aligned} \frac{\Gamma(n+c)}{\Gamma(n)} &\approx n^c \left[1 + \frac{c(c-1)}{2n} + \frac{c(c-1)(c-2)(3c-1)}{24n^2} \right. \\ &\quad \left. + \dots \right], \end{aligned} \quad (5)$$

with $n=m/\delta^2$ and $c=1/\delta$, $2/\delta$ successively in Table II gives

$$\left(\frac{\text{Standard deviation}}{\text{Mean}} \right)^2 = \frac{1}{m} + \frac{(1-\delta^2)}{2m^2} + \dots$$

When δ is close to unity or m is large, the series can be truncated from the second term. Hence,

$$\frac{\text{Standard deviation}}{\text{Mean}} \approx \frac{1}{\sqrt{m}}.$$

Thus, in the 3Γ model m is the regularity factor when δ is close to unity or m is large. If both models are fitted to the same set of data, the m of the 3Γ model will be nearly equal to the m of the 2Γ model. This correspondence can be observed for the Poisson tessellation case in Table III. This correspondence is shown for hard-disk and hard-sphere sys-

tems in Sec. IV. From the regularity factors in Table III, it can be noted that the Poisson tessellation becomes more regular as the dimension increases.

III. MAXIMUM INFORMATION ENTROPY (MAX-ENT) FORMALISM

The *uncertainty* or the *information entropy*^{27,28} of a discrete distribution is $s_I = -k_B \sum P_i \log P_i$, where P_i is the probability of the i th outcome and the summation is over all the outcomes. The analogous definition for a continuous distribution $f(x)$ is $s_I = -k_B \int f(x) \log[f(x)] dx$, where the integration is over the full domain of x . As an illustration, consider the uncertainty of a coin toss, $s_I = -k_B [p \log p + q \log q]$, where p is the probability of a head and $q = 1 - p$ is the probability of a tail. It can be easily seen that the uncertainty of the outcome is maximum when $p = q = 1/2$. This physically means that when $p = q = 1/2$ one would need maximum information (the complete knowledge of the dynamics of a toss and the initial conditions) to predict the outcome. One could as well arrive at this value of p by the principle of equal *a priori* probability (PEAP), which assigns an equal probability for all the outcomes when no other information is available. However, in a complex situation where PEAP does not apply or the complete understanding of the system is lacking, the max-ent formalism is a powerful method to estimate the most probable distribution²⁹ For example, Engelman *et al.*³⁰ have derived the size distribution of fragments in a disintegration process (say, blasting) showing good agreement with experimental observations, using the max-ent formalism with the energy and volume constraints on the fragments.

In general, the information entropy need not be related to the thermodynamic entropy, since the system under consideration itself need not be in equilibrium, as in the above-mentioned disintegration process. However, if the system is in thermodynamic equilibrium and if the distribution under consideration contains all the relevant information (to the desired level of description), then the information entropy will be identical to the thermodynamic entropy. For example, in a monatomic fluid of N particles in a container of constant volume and temperature, the information entropy defined on the N -particle position and velocity distribution function, $f_N(\mathbf{r}_1, \dots, \mathbf{r}_N, \mathbf{v}_1, \dots, \mathbf{v}_N)$, where \mathbf{r}_i and \mathbf{v}_i are the position and velocity of the i th particle, respectively, is identical to the thermodynamic entropy.³¹ Now, if we employ PEAP for the energy states (i.e., states with identical energies having identical probabilities), then $f_N(\mathbf{r}_1, \dots, \mathbf{v}_N) = f[E(\mathbf{r}_1, \dots, \mathbf{v}_N)]$ and $f(E)$ contains all the information about the system, up to the level of macroscopic averaging. Hence, the information entropy defined on $f(E)$ is also identical to the thermodynamic entropy, even though the microscopic information content of $f(E)$ is much less than that of $f_N(\mathbf{r}_1, \dots, \mathbf{v}_N)$.²⁸

Now, the uncertainty or the information entropy defined on the cell volume distribution is

$$s_I = -k_B \int_{v_c}^{\infty} f(v) \log[f(v)] dv.$$

Transforming the independent variable to the free volume $v_f = v - v_c$ gives

$$s_I = -k_B \int_0^{\infty} f(v_f) \log[f(v_f)] dv_f. \quad (6)$$

This definition of information entropy employs the equality of all the cell volumes as the measure of order. At the regular close packing, all the cell volumes are identical and the free volume distribution is a Dirac delta distribution and hence s_I is negative infinity; i.e., we need minimum information (the crystal's unit cell) to construct these configurations. Using the method of the Lagrange multipliers, with the mean free volume condition ($v_f = \bar{v} - v_c$), it can be easily shown that an exponential free volume distribution has a maximum information entropy. From Sec. II, we know that the Poisson tessellation (ideal gas) cell volume distribution is not exponential. The Poisson configuration does not maximize s_I because these configurations could be easily constructed using a uniform random number generator. We might speculate that the DRP (or the jammed packings in general) might have an exponential free volume distribution, since we need maximum information (all the particle positions) to construct the configuration. The algorithm we have used produces dense random structures with nearly but not exactly exponential free volume distribution; further details are in Sec. IV.

The gamma distributions contain the exponential distribution as a limiting case ($m = 1$ for 2Γ model and $\delta, m = 1$ for 3Γ model). Hence, it is obvious that even within these two families of distributions, the exponential distribution maximizes the information entropy. However, we show the explicit analysis for the 2Γ model, since we require an intermediate result for Sec. V. The 2Γ model, on integration, gives

$$\frac{s_I}{k_B} = \log[\bar{v}(1-y)] - (m-1)\Psi(m) + \log[\Gamma(m)] - \log(m) + m, \quad (7)$$

where $\Psi(\cdot)$ is the digamma function. Here, we have used a standard integral from Gradshteyn and Ryzhik,³²

$$\int_0^{\infty} x^{m-1} e^{-\alpha x} \log(x) dx = \frac{\Gamma(m)}{\alpha^m} [\Psi(m) - \log(\alpha)], \quad (8)$$

and then eliminated α using Eq. (4). In the 2Γ model, the free parameter m is a function of y and the type of structures (thermodynamic or otherwise), hence s_I is a functional of m . To maximize s_I , we set

$$\frac{\partial}{\partial m} \left(\frac{s_I}{k_B} \right) = (m-1) \left(\frac{1}{m} - \Psi^{(1)}(m) \right) = 0, \quad (9)$$

Here, $\Psi^{(n)}(\cdot)$ are the polygamma functions. It can be easily checked that the solution $m = 1$ is a maximum, using $\Psi^{(1)}(1) = \pi^2/6$. We will pursue the connection of s_I with the thermodynamic entropy in Sec. V; for use therein we rewrite Eq. (7) as $s_I/k_B = \log[\bar{v}(1-y)] + \phi(m)$, where $\phi(m) = -(m-1)\Psi(m) + \log[\Gamma(m)] - \log(m) + m$. Setting $y = 0$ gives the information entropy for the ideal gas at the same specific volume as $s_I^0/k_B = \log(\bar{v}) + \phi(m_0)$. Then, the excess information entropy is

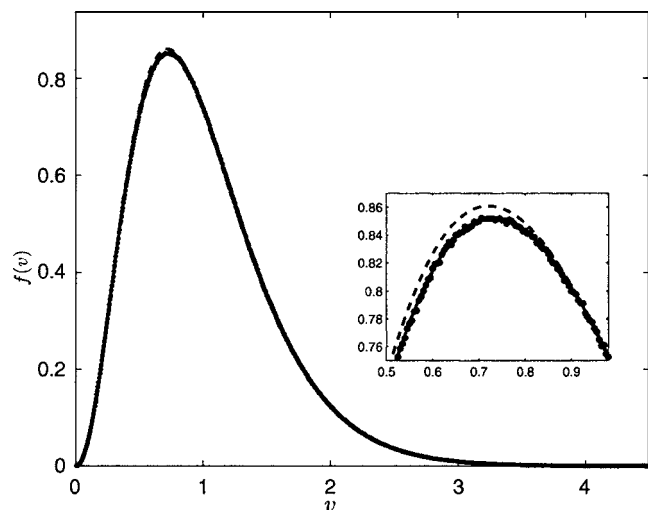


FIG. 3. 2D Poisson tessellation cell area distribution. Simulation data (●), 2Γ model (---), and 3Γ model (—). Averaged over 10^5 configurations of 1000 points with periodic boundary conditions (PBC). The best-fit parameter values are given in Table III. The cell volume is scaled by the specific volume.

$$\frac{S_I^E}{k_B} = \log(1 - y) + \phi(m) - \phi(m_0). \quad (10)$$

IV. SIMULATION RESULTS

The cell volume distribution for the 2D Poisson tessellation is given in Fig. 3. The 2Γ model has a positive error at the peak (shown in inset) and a compensating negative error near the origin. The 3Γ model gives a better fit, however, at the cost of an additional parameter. This statistical superiority of the 3Γ model over the 2Γ model holds for the entire density range for both hard-disk and hard-sphere structures, as shown in the auxiliary material,³³ by a mean-square error analysis.

We have studied three types of hard-disk structures: NVE-MC, NPT-MC, and swelled random structures. The NVE-MC configurations are made with 50% success rate; i.e. the amplitude of the random trial displacement is adjusted such that 50% of the trials lead to nonoverlapping configurations. The NPT-MC algorithm is from Wood.³⁴ The results from NPT configurations are ascribed to their average ν . The swelled random structures are generated using a Monte Carlo (MC) adaptation of Woodcock's³⁵ algorithm: swell the nearest neighbors till they touch each other, give random trial steps (with say 50% success rate as in NVE-MC) for all the particles and continue the swelling process until the desired ν is attained. If the success rate is low, the large trial displacements tend to equilibrate the local structures. However, if the success rate is high, the trial displacements are small and the swelling process locks the particles into random structures. The effect of the success rate on the resultant structures is studied below.

Compare the degree of fit for the NVE and the swelled random structures, both at $\nu=0.82$ in Figs. 4 and 5 (after ignoring the greater scatter in the random structure data due to lesser averaging). A bimodal $f(\nu)$ (as in Fig. 5) indicates the existence of dense and lean regions due to the formation

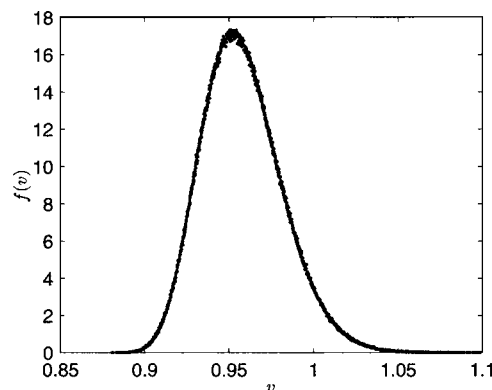


FIG. 4. Cell volume distribution for hard-disk NVE structure at $\nu=0.82$. Simulation data (●), 2Γ model (---), and 3Γ model (—). Averaged over 10 000 configurations of 256 hard-disks with PBC.

of crystallites. The most appropriate method to quantify the crystallite concentration in a random hard-disk configuration is to classify the hard-disks as solidlike or fluidlike based on the bond orientational order parameter³⁶ and compute the fraction of solidlike disks. This analysis for the swelled random structures is in progress and will be reported separately. Alternatively, one could monitor the population of hexagons as a measure of crystallite concentration, as shown in our recent work.³⁷ Local crystallization, however, is typical of random packing algorithms, especially in the hard-disk system due to the lack of geometric frustration.²⁴ For example, the cell volume distribution in Fig. 62 of Glaser and Clark,³⁶ in addition to the two distinct modes, has a large-volume tail due to the grain boundaries around the crystallites. Due to such structural inhomogeneities caused by the DRP algorithm, the gamma distributions give a poor fit near ν_{DRP} (see auxiliary material³³) and hence the max-ent predictions are approached but not exactly realized in the following results. The good performance of the 3Γ model for the *homogeneous* thermodynamic structures across the entire ν range (see auxiliary material³³) and the approach to the max-ent predictions make us speculate that an ideal DRP algorithm producing homogeneous structures might satisfy the max-ent predictions.

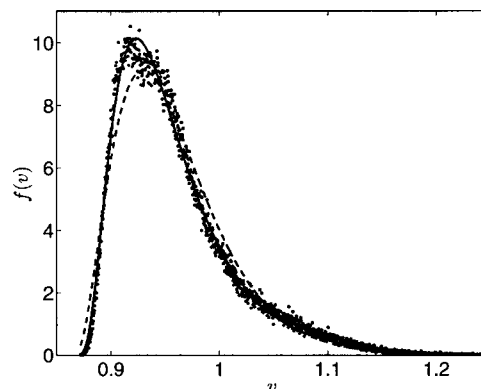


FIG. 5. Cell volume distribution for hard-disk swelled random structure at $\nu=0.82$. Simulation data (●), 2Γ model (---), and 3Γ model (—). Averaged over 1000 configurations of 256 hard-disks with PBC. Note the bimodal nature of the distribution.

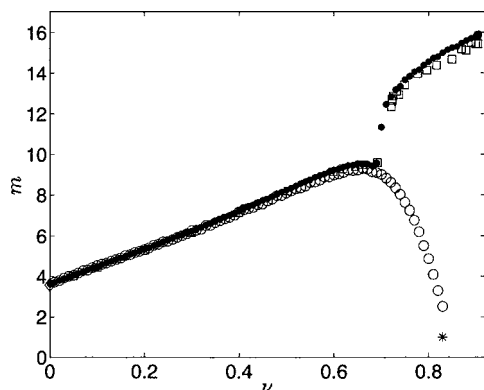


FIG. 6. The 2Γ model m values for hard-disk structures. NVE-MC (\bullet), NPT-MC (\square), swelled random at 50% success rate (\circ), Poisson limit (\diamond), and max-ent prediction at dense random-packing limit (*). Averaged over 10 000 configurations for NVE/NPT and 1000 configurations for swelled random structures of 256 hard-disks with PBC.

The 2Γ model m values for the various hard-disk configurations considered are given in Fig. 6, from which we observe the following.

- For thermodynamic structures (NVE and NPT) as ν increases, cells become more regular and hence m increases. Due to the onset of order at the freezing transition, the thermodynamic structures have a sharp increase in m . The thermodynamic structures terminate at the regular close packing.
- The NPT and NVE structures are identical; it can be explained as follows: Since the radial distribution function of an NPT ensemble at its *average* ν is identical to that of an NVE ensemble at the same ν , the local neighborhoods being identical, the cell volume distributions are identical. The differences between NVE and NPT structures seen on the solid branch may be ascribed to the limited sampling.
- For $\nu < \nu_F$ the swelled random structures become more regular (i.e., m increases) as ν increases, and this behavior is identical to that of the thermodynamic fluid structures. However, for $\nu > \nu_F$ the swelled random structures become more irregular (i.e., m decreases) with

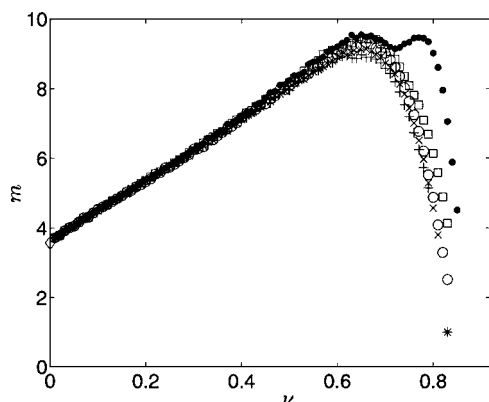


FIG. 7. Hard-disk swelled random structures for different success rates. Success rates of 10% (\bullet), 30% (\square), 50% (\circ), 70% (\times), and 90% ($+$); Poisson limit (\diamond); and max-ent prediction at dense random packing limit (*). Averaged over 1000 configurations of 256 hard-disks with PBC.

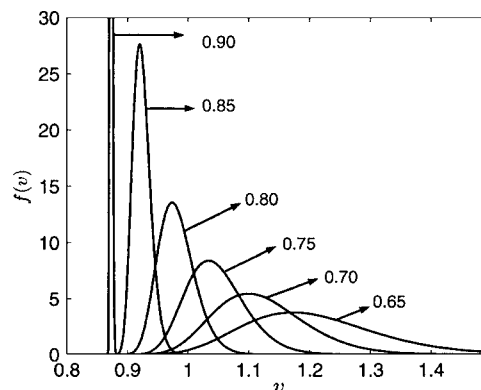


FIG. 8. Hard-disk thermodynamic configurations. For $\nu > \nu_F$ as ν increases the cell volume distribution becomes narrow, and at ν_c it degenerates to a Dirac delta distribution located at ν_c . All lengths are scaled by the diameter of a disk.

increase in ν and terminate at the dense random-packing limit. This behavior is drastically different from that of the thermodynamic solid structures and can be clearly seen by comparing Figs. 8 and 9.

The swelled random structures can be made with different success rates. As mentioned earlier, at low success rates the large trial displacements tend to equilibrate the local non-equilibrium structures, and hence the m value approaches that of the thermodynamic structures at the same ν . This can be observed in Fig. 7, for $\nu > \nu_F$ swelled random structures are with 10% success rate. Figure 7 shows that with increasing success rates, all the structures lie on a unique branch of dense random structures. At any success rate, attaining a desired ν through a relay of lower ν configurations with small $\Delta\nu$ and reinitializing the random number generator at each halt avoid the build up of structural signatures due to the random number generator algorithm. Structures made in a small $\Delta\nu$ relay (for Fig. 7 $\Delta\nu=0.01$) are independent of the success rates. Structures made in a large $\Delta\nu$ relay (say $\Delta\nu>0.1$) depend on the success rates, and these structures have an m value lesser than that of the thermodynamic structures at the same ν . This method can be used to generate

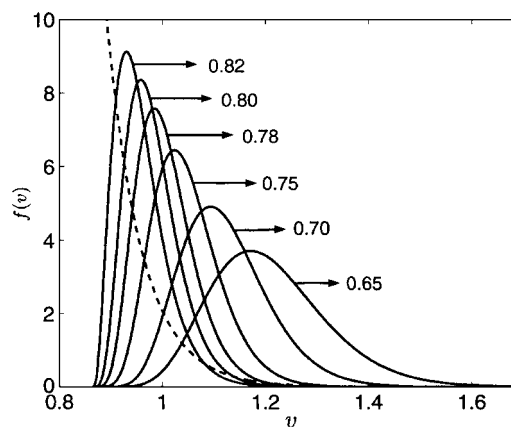


FIG. 9. Hard-disk swelled random configurations. For $\nu > \nu_F$ as ν increases, the ratio of standard deviation to mean ($1/\sqrt{m}$) of the cell volume distribution increases. All lengths are scaled by the diameter of a disk. The max-ent prediction is shown by the broken line (---).

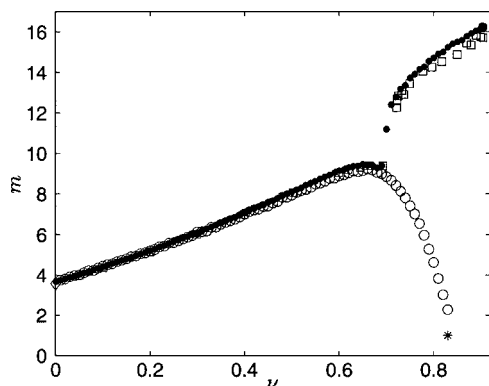


FIG. 10. 3Γ model m for hard-disk structures. NVE-MC (\bullet), NPT-MC (\square), swelled random structures at 50% success rate (\circ), Poisson limit (\diamond), and max-ent prediction at dense random-packing limit (*). Averaging as in Fig. 6.

structures having an m value lower than that of the thermodynamic structures. Structures having an m value greater than that of the thermodynamic structures can be made by shrinking the disk diameter of denser thermodynamic structures.

The m and δ values for the 3Γ model for the free volume distribution of hard-disk structures are given in Figs. 10 and 11. From Figs. 6 and 10 it is observed that the 3Γ model m compares well with the 2Γ model m , within a few percent difference, when m is large or δ is close to unity. In Fig. 11, it is interesting to note that the swelled random structures approach the max-ent prediction ($\delta=1$) at the dense random-packing limit with drastic changes. These drastic trend changes are not an artifact of curve fitting, since we got identical results with different optimizer algorithms (Nelder-Mead and Gauss-Newton) and different initial estimates. The optimizer, after the initial excursion, settles into a nearly constant m trajectory (that which corresponds to the regularity factor) on the error surface (a function of m and δ) and searches for a δ value which minimizes the error along this trajectory. The error surface does not have multiple local minima in the working range of the parameters (m ranging from 1 to 35 and δ ranging from 0.1 to 2), as seen from Fig. 12. Since the error magnitudes vary widely for the state

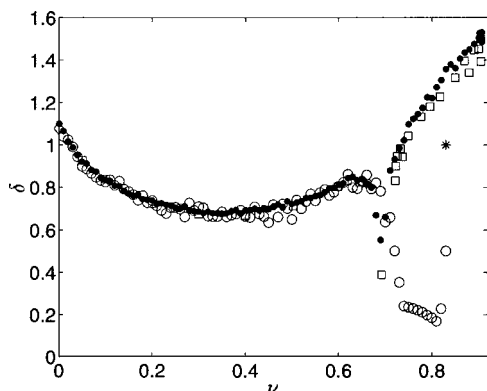


FIG. 11. 3Γ model δ for hard-disk structures. NVE-MC (\bullet), NPT-MC (\square), swelled random structures at 50% success rate (\circ), Poisson limit (\diamond), and max-ent prediction at dense random-packing limit (*). Averaging as in Fig. 6.

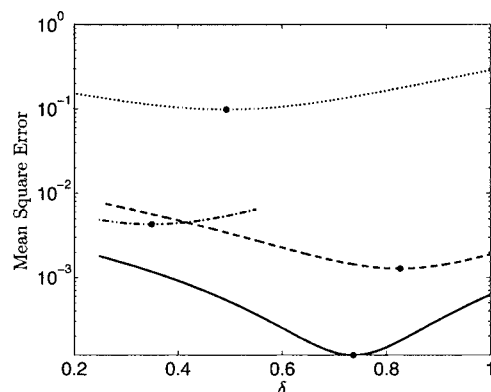


FIG. 12. Error in 3Γ model as a function of δ along constant m trajectories, for hard-disk swelled random structures at 50% success rate and $\nu=0.55$ (—, $m=8.4981$), $\nu=0.65$ (---, $m=9.1465$), $\nu=0.73$ (-.-, $m=8.1272$), and $\nu=0.83$ (\cdots , $m=2.2827$). The δ at the minimum error (\bullet) are the optimized values reported in Fig. 11.

points considered, in Fig. 12 a logarithmic scale is used for the y axis. Though some of the curves appear flat in this scale, the minima are distinct in the linear scale.

Now we present the analogous results in three dimensions (3D). The three-dimensional (3D) Poisson tessellation cell volume distribution is given in Fig. 13. The approach of the swelled random hard-sphere structures towards the max-ent predictions is less satisfactory than that of the hard-disk system; even though the trend in m (Fig. 15) is towards unity, the trend in δ (Fig. 16) is away from unity as DRP is approached. The parameter m in the 2Γ and 3Γ models are nearly identical inspite of δ being nearly 2, since the m values are large.

V. CONFIGURATIONAL ENTROPY

The Appendix gives the thermodynamic definition of the configurational properties. In the context of *regular* cell theory, Kirkwood³⁸ showed that the configurational entropy can be partitioned as $s_{\text{conf}}=s_{\text{cell}}+s_{\text{com}}$, where s_{cell} is the cellular entropy arising due to the single occupancy of the regular cells and s_{com} is the communal entropy arising due to the multiple occupancy of the regular cells. In the context of the free volume theory of glasses and supercooled liquids,

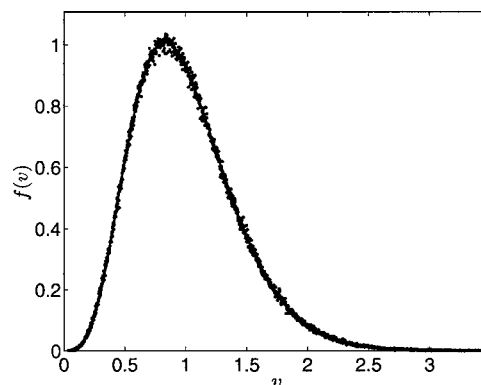


FIG. 13. 3D Poisson tessellation cell volume distribution. Simulation data (\bullet), 2Γ model (---) and 3Γ model (—). Averaged over 1000 configurations of 1000 points with PBC. The best-fit parameter values are given in Table III. The cell volume is scaled by the specific volume.

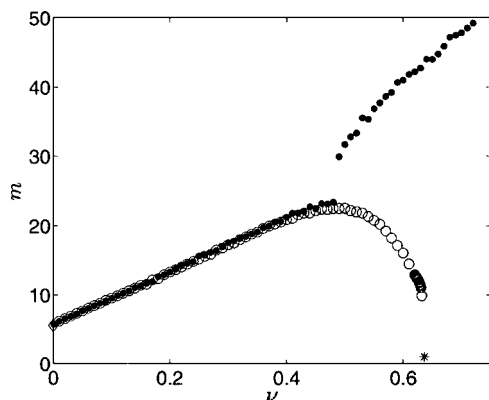


FIG. 14. The 2Γ model m for hard-spheres. NVE-MC (●), swelled random structures at 50% success rate (○), Poisson limit (◇), and max-ent prediction at dense random-packing limit (*). Averaged over 1000 configurations of 256 hard-spheres with PBC.

Cohen and Grest^{39–41} assumed that the above partitioning holds as well for the irregular cellular structure defined by the Voronoi polyhedra of the particles. They introduced the expression $s_{fv} = -k_B \int f(v) \log[f(v)] dv$, in analogy with the entropy of mixing, where $f(v)$ is the Voronoi cell volume distribution. (Here, we use the notation s_{fv} instead of s_{cell} , since s_{fv} corresponds to the entropy associated with Voronoi free volume distributions). To validate the ansatz, we independently compute and compare the left- and right-hand sides of the ansatz for hard-disk and hard-sphere systems. The right-hand side is computed from the free volume distributions discussed in Sec. IV and the left-hand side is computed independently from the thermodynamic data (details below). To the best of our knowledge, such an analysis is not reported for any system.

For the Voronoi free volume or cellular entropy we take the Cohen-Grest expression as

$$s_{fv} = -\lambda k_B \int_{v_c}^{\infty} f(v) \log[f(v)] dv, \quad (11)$$

allowing a density-independent proportionality constant λ (if λ is density dependent, the ansatz is of negligible value); its necessity will be clear below. Cohen and Grest³⁹ define the communal entropy, based on the existence of liquid clusters,

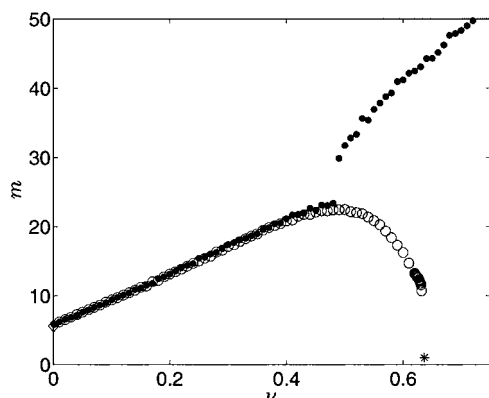


FIG. 15. 3Γ model m for hard-sphere structures. NVE-MC (●), swelled random structures at 50% success rate (○), Poisson limit (◇), and max-ent prediction at dense random-packing limit (*). Averaging as in Fig. 14.

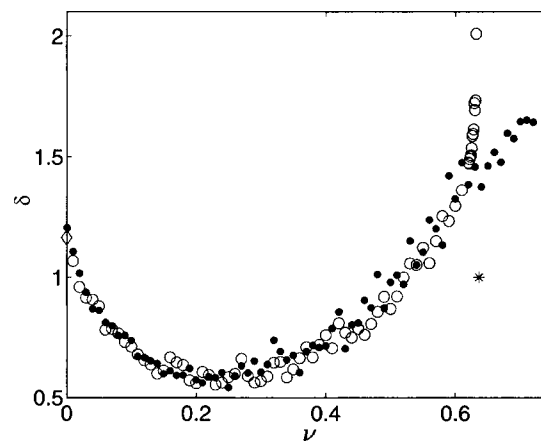


FIG. 16. 3Γ model δ for hard-sphere structures. NVE-MC (●), swelled random structures at 50% success rate (○), Poisson limit (◇), and max-ent prediction at dense random-packing limit (*). Averaging as in Fig. 14.

as “the entropy associated with the accessibility of all of the configurational volume within the finite liquid clusters and within the infinite cluster, when present.” For densities above the freezing density very few fluid clusters exist, and hence the communal entropy is a negligible fraction of the configurational entropy. In the regular close-packed limit, the communal entropy is zero and hence the configurational entropy is purely cellular. We identify λ by comparing the cellular entropy with the configurational entropy near the regular close packing. For ease of comparison, we express all entropies as excess entropies, with the reference ideal gas at the same specific volume. Now, the above condition is expressed as

$$\lim_{\nu \rightarrow \nu_c} s_{\text{conf}}^E = s_{fv}^E, \quad (12)$$

and the ansatz [Eq. (11)] is rewritten as $s_{fv}^E = \lambda s_I^E$, where the s_I^E is the excess information entropy. Using Eq. (10) for s_I^E we get

$$\frac{s_{fv}^E}{k_B} = \lambda \log(1 - y) + \lambda [\phi(m) - \phi(m_0)]. \quad (13)$$

To compute s_{conf}^E we use the thermodynamic identity (proof in the Appendix) $s_{\text{conf}}^E = s_v^E$, where s_v^E is the excess entropy of a fluid, with the reference ideal gas at the same specific volume. For hard-spheres s_v^E is computed from the equation of state (EOS) as⁴²

$$\frac{s_v^E}{k_B} = - \int_0^y \frac{Z-1}{y} dy, \quad (14)$$

where $Z = p\bar{v}/(k_B T)$ is the compressibility factor. Differentiating Eq. (14) with respect to y and rearranging gives

$$Z = 1 - y \frac{d}{dy} \left(\frac{s_v^E}{k_B} \right). \quad (15)$$

Using Eqs. (12), (13), and (15) and the identity $s_{\text{conf}}^E = s_v^E$ gives

TABLE IV. EOS and excess entropy equations plotted in Figs. 17 and 18.

System	$Z, \frac{s_v^E}{k_B}$ and notes	Reference for EOS
HD/HS virial expansion	$Z = 1 + B_2\nu + B_3\nu^2 + B_4\nu^3 + \dots$ $\frac{s_v^E}{k_B} = -\left(B_2\nu + \frac{B_3}{2}\nu^2 + \frac{B_4}{3}\nu^3 + \dots\right)$ B_2 to B_8 in Table V	van Rensburg (Ref. 56)
HD MD fluid data fit	$Z = \frac{1 + A\nu + B\nu^2}{(1-\nu)^2}$ $\frac{s_v^E}{k_B} = -\frac{(1+A+B)\nu}{(1-\nu)} - (B-1)\log(1-\nu)$ $A=0.05833, B=0.01267$	Maeso and Solana (Ref. 57)
HD MD solid data fit	$Z = 2/a + 1.90 + 0.67a + 1.5a^2$ where $a = \frac{\bar{v} - \nu_c}{\nu_c} = 1/y - 1$	Young and Alder (Ref. 58)
HS MD fluid data fit or the Carnahan-Starling EOS	$Z = \frac{1 + \nu + \nu^2 - \nu^3}{(1-\nu)^3}$ $\frac{s_v^E}{k_B} = \frac{-\nu(4-3\nu)}{(1-\nu)^2}$	Carnahan and Starling (Ref. 59)
HS MD solid data fit	$Z = 3/a + 2.566 + 0.55a - 1.19a^2 + 5.95a^3$ a as above	Young and Alder (Ref. 58)
HD/HS composite EOS	$\frac{s_v^E}{k_B} = -\int_0^\nu \frac{Z_f - 1}{\nu} d\nu$ for $\nu < \nu_F$ $\frac{s_v^E}{k_B} = -\int_0^{\nu_F} \frac{Z_f - 1}{\nu} d\nu - \frac{\Delta s_F}{k_B} - \int_{\nu_F}^\nu \frac{Z_s - 1}{\nu} d\nu$ for $\nu > \nu_F$ $\Delta s_F/k_B = 0.36$ for HD $\Delta s_F/k_B = 0.92$ for HS	Z_f is fluid fit given above Z_s is solid fit given above
HD/HS cell theory	$Z = (1 - y^{1/D})^{-1}$ $\frac{s_v^E}{k_B} = D \log(1 - y^{1/D})$ $D = \text{dimension.}$	Wood (Ref. 60)

$$\lim_{\nu \rightarrow \nu_c} Z = \frac{\lambda y}{1-y} + 1 - \lambda y \left(\frac{\partial \phi}{\partial m} \right) \left(\frac{dm}{dy} \right). \tag{16}$$

Hoover⁴³ show that the form of the dense hard-sphere solid EOS is

$$Z = \frac{D}{a} + c_0 + c_1 a + c_2 a^2 + \dots, \tag{17}$$

where $a = (\bar{v} - \nu_c) / \nu_c = (1 - y) / y$ is the dimensionless excess free volume (see Table IV). Comparing Eqs. (16) and (17), and noting from Figs. 6 and 14 that (dm/dy) does not diverge at $y=1$, we identify $\lambda = D$. Before proceeding further, we would like to emphasize the wide implications of this identification.

TABLE V. Virial coefficients for hard-disk and hard-sphere fluids, from Sanchez (Ref. 47).

n	HD B_n	HS B_n
2	2	4
3	3.128 017 8	10
4	4.257 854	18.364 77
5	5.336 897	28.224 5
6	6.362 6	39.74
7	7.351	53.54
8	8.338	70.8

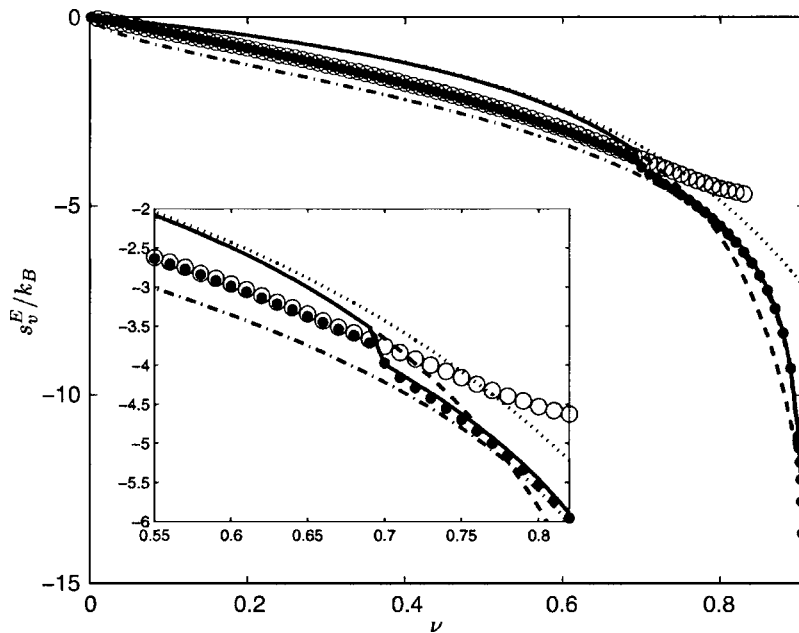


FIG. 17. Hard-disk excess entropy prediction from m data. Voronoi NVE (\bullet), Voronoi, swelled random structures at 50% success rate (\circ), virial EOS (\cdots), fluid molecular-dynamics (MD) fit ($---$), regular cell theory ($- \cdot -$), and composite EOS ($-$). The Voronoi prediction is obtained by using the m data from Fig. 6 in Eq. (11) with $\lambda=2$. The equations for the other data are given in Table IV.

- The low-density and high-temperature limit of any system of particles with short-ranged interaction, is identical to the low-density limit of hard-spheres. Hence this identification holds in the ideal gas limit of any system of particles. But then λ is density independent, hence the identification holds for any system at any density. This generality is anticipated since λ depends only on the dimension of the system.
- It should be noted that the information of the particular form used to fit the free volume distribution (in this work the gamma distribution) is contained in ϕ of Eq. (16). And this information is irrelevant for the identification $\lambda=D$ as long as it does not contribute a divergent term to the right-hand side of Eq. (16) at $y=1$. Hence this identification is exact, even though the gamma representations are merely good approximations. However, note that the definition of the free volume as $v_f = v - v_c$ is crucial in recovering the thermodynamic singularity correctly at the regular close packing. Any other definition of free volume like $v_f = v - v_p$, where v_p is the particle volume, or $v_f = v - v_{\text{opt}}$, where v_{opt} is some optimized minimum cell volume (used in Hanson⁴⁴), will not recover the thermodynamic singularity at the regular close packing when used with the Cohen-Grest ansatz.
- With the identification $\lambda=D$, the free volume or cellular entropy is first-order homogeneous in D . Note that the last two terms on the right-hand side of Eq. (A3), arising from the integration of momenta, are also first-order homogeneous in D . This is a general behavior, as shown by the following simple model. Consider a system of N independent hard-spheres rattling inside some volume and suppose that, at any instant, the direction of displacement is the only relevant variable. Then, at any instant, an independent sphere can displace in $\pm x$, $\pm y$, or $\pm z$ directions; hence it has 2^D states, where $D=3$. The number of states available to the system is $\Omega=(2^D)^N$

$=2^{ND}$. Hence, the entropy, $S=k_B \log \Omega=Nk_B D \log 2$, is first-order homogeneous in D . This behavior is not observed in the Ising model since the number of states is identically two (up and down) for an independent spin in any dimension. But systems in which the number of states of an independent particle increases with D as 2^D have an entropy first-order homogeneous in D .

- For static powders, the communal entropy is identically zero. Hence, the ensemble-averaged entropy for similarly prepared powders is purely cellular. Hence, with the identification $\lambda=D$ in Eq. (11), the entropy of static powders is fully characterized by the free volume distributions. Even if the gamma representations are a poor fit for the free volume distributions, a numerical integration of the right-hand side of Eq. (11) could be effected.

Now we show the validity of the identification $\lambda=D$ for

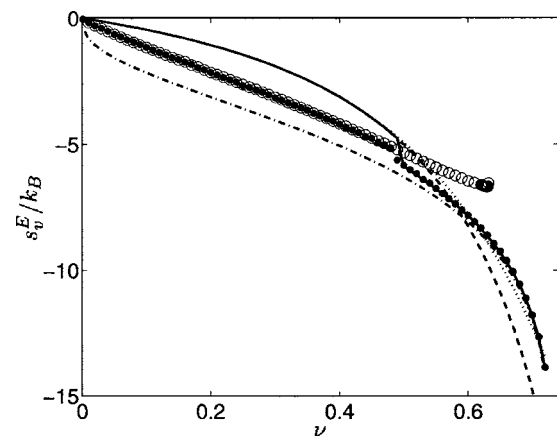


FIG. 18. Hard-sphere excess entropy prediction from m data. Voronoi-NVE (\bullet), Voronoi, swelled random structures at 50% success rate (\circ), virial EOS (\cdots), fluid MD fit ($---$), regular cell theory ($- \cdot -$), and composite EOS ($-$). The Voronoi prediction is obtained by using the m data from Fig. 14 in Eq. (11) with $\lambda=3$. The equations for the other data are given in Table IV.

each dimension separately. In the hard-rod system there is no solid-fluid transition. Hence, a hard-rod configuration at any ν is a *dilute* solid and not a fluid. Since there are no fluid clusters in the hard-rod system, its communal entropy (in the Cohen-Grest sense) is identically zero and the configurational entropy is purely cellular. From Sec. II, for hard-rods we have $m=m_0=2$ and hence $dm/dy=0$. Using these with $\lambda=1$ in Eqs. (16) and (13) we recover the exact results: Tonk's EOS⁴⁵ $Z=(1-y)^{-1}$ and $s_v^E/k_B=\log(1-y)$. Thus, for the hard-rod system, Eq. (11) is exact with $\lambda=1$.

For the hard-disk and hard-sphere systems, we compute the excess entropy $s_{\text{conf}}^E (=s_v^E)$ from the different EOS reported in literature, using Eq. (14). These expressions are given in Table IV. The hard-disk and hard-sphere virial coefficients, required in Table IV, are given in Table V. After the freezing transition, the configurational entropy should be slightly greater than the free volume or cellular entropy, since the communal entropy is a small non-negative contribution. The equality holds in the limit of regular close packing, where the communal entropy vanishes. Using the Voronoi m data for the hard-disk and hard-sphere systems from Figs. 6 and 14, on the right-hand side of Eq. (11) with $\lambda=2$ and 3, respectively, we get the Voronoi estimates of the free volume or cellular entropy. These results are plotted in Figs. 17 and 18. From these figures, we see that the free volume or cellular entropy matches with the configurational entropy for the thermodynamic solid phase, except for the small non-negative communal entropy (see Fig. 17 inset). Note that, in these figures, the vertical distance between the composite EOS curve and the NVE-MC Voronoi data is the excess communal entropy. For the hard-sphere composite EOS equation in Table IV, we have taken the entropy change during freezing, $\Delta s_F/k_B$ as 0.92 (instead of the approximate value of 1.16 given in Table I), so that the excess communal entropy is non-negative. This revision is justified as follows: By comparing the entropy difference between an ideal gas (with the configurational integral $Q_{\text{conf}}^0 = V^N/N! = \bar{v}^N N^N/N!$) and a regular cellular solid at the same specific volume ($Q_{\text{conf}} = \bar{v}^N$), it can be easily seen that $\Delta s_F/k_B$ for *smooth* elastic hard hyperspheres cannot be greater than unity.

VI. CONCLUSIONS

The Voronoi free volume distributions of the hard-disk and hard-sphere systems are well represented by a two-parameter (2Γ) or a three-parameter (3Γ) gamma distribution (Table II). After imposing the specific volume constraint m is the free parameter in the 2Γ model and m, δ are the free parameters in the 3Γ model. It is shown that parameter m in the 2Γ and the 3Γ models is the regularity factor. For the thermodynamic structures, the regularity factor increases with increasing density and it increases sharply across the freezing transition, in response to the onset of order. The regularity factor also distinguishes between the dense thermodynamic structures and dense random structures. The maximum information entropy formalism predicts that the free volume distribution at the dense random-packed state is an exponential distribution. This prediction seems to be approached, but not exactly reached, due to the structural inho-

mogeneities induced by the dense random-packing algorithm. This suggests a precise definition for dense random packing as the packing at which the information entropy of the Voronoi free volume distribution is maximized. The connection between the free volume entropy and the thermodynamic entropy was examined in the limit of regular close packing where the communal part of the entropy vanishes. We find that the Cohen-Grest expression relating the thermodynamic and the free volume entropy is exact for hard-rod system, and a correction factor equal to the dimension of the system is necessary for hard-disk and hard-sphere systems. This correction factor is anticipated if the number of states of an independent particle increases with the dimension of the system, D , as 2^D .

APPENDIX: CONFIGURATIONAL PROPERTIES

The canonical partition function for N indistinguishable classical particles of mass m in D dimensions is

$$Q = \left(\frac{2\pi mk_B T}{h^2} \right)^{DN/2} Q_{\text{conf}},$$

where Q_{conf} is the configurational integral,

$$Q_{\text{conf}} = \frac{1}{N!} \int_V \cdots \int_V \exp(-\beta U) d\mathbf{r}_1 \cdots d\mathbf{r}_N,$$

and $U(\mathbf{r}_1, \dots, \mathbf{r}_N)$ is the potential energy of the system in the configuration $\{\mathbf{r}_1, \dots, \mathbf{r}_N\}$. The Helmholtz free energy is $F = -k_B T \log Q$ and the entropy is

$$S = - \left(\frac{\partial F}{\partial T} \right)_{N,V} = k_B \log Q + k_B T \left(\frac{\partial \log Q}{\partial T} \right)_{N,V}. \quad (\text{A1})$$

The configurational analogs⁴⁶ are defined as $F_{\text{conf}} = -k_B T \log Q_{\text{conf}}$ and

$$\begin{aligned} S_{\text{conf}} &= - \left(\frac{\partial (F_{\text{conf}})}{\partial T} \right)_{N,V} \\ &= k_B \log(Q_{\text{conf}}) + k_B T \left(\frac{\partial \log(Q_{\text{conf}})}{\partial T} \right)_{N,V}. \end{aligned} \quad (\text{A2})$$

From Eqs. (A1) and (A2), we get

$$S = S_{\text{conf}} + \frac{D}{2} N k_B \log \left(\frac{2\pi mk_B T}{h^2} \right) + \frac{D}{2} N k_B. \quad (\text{A3})$$

Replacing S and S_{conf} , respectively, with S^0 and S_{conf}^0 , we get the entropy of the ideal gas. Then the excess entropy $S_v^E = S_{\text{conf}}^E$. Note that the reference ideal gas has the same specific volume as the fluid under consideration due to the constancy of N and V in the canonical ensemble. For the ideal gas with $Q_{\text{conf}}^0 = V^N/N!$ and Stirling's approximation, $\log N! = N \log N - N$, we have $S_{\text{conf}}^0 = N k_B + N k_B \log v$.

¹G. Voronoi, J. Reine Angew. Math. **134**, 198 (1908).

²D. C. Rapaport, Mol. Phys. **48**, 23 (1983).

³F. Aurenhammer, ACM Comput. Surv. **23**, 345 (1991).

⁴A. Okabe, B. Boots, and K. Sugihara, *Spatial Tessellations: Concepts and Applications of Voronoi Diagrams* (Wiley, New York, 1992).

⁵G. Schliecker, Adv. Phys. **51**, 1319 (2002).

⁶B. N. Boots, Metallography **15**, 53 (1982).

⁷H. X. Zhu, S. M. Thorpe, and A. H. Windle, Philos. Mag. A **81**, 2765

- (2001).
- ⁸L. Oger, A. Gervois, J. P. Troadec, and N. Rivier, *Philos. Mag. B* **74**, 177 (1996).
- ⁹A. Bondi, *J. Phys. Chem.* **58**, 929 (1954).
- ¹⁰L. Lepori and P. Gianni, *J. Solution Chem.* **29**, 405 (2000).
- ¹¹J. C. McGowan and A. Mellors, *Molecular Volumes in Chemistry and Biology Applications Including Partitioning and Toxicity* (Ellis Harwood, Chichester, UK, 1986).
- ¹²W. G. Hoover, N. E. Hoover, and K. Hanson, *J. Chem. Phys.* **70**, 1837 (1979).
- ¹³H. Reiss, *J. Phys. Chem.* **96**, 4736 (1992).
- ¹⁴D. K. Doolittle, *J. Appl. Phys.* **22**, 1471 (1951).
- ¹⁵*The Physics of Glassy Polymers*, edited by R. N. Haward (Applied Science Publishers, London, 1973).
- ¹⁶S. Matsuoka and A. Hale, *J. Appl. Polym. Sci.* **64**, 77 (1997).
- ¹⁷T. Yamamoto and H. Furukawa, *J. Appl. Polym. Sci.* **80**, 1609 (2001).
- ¹⁸G. Consolati, M. Levi, L. Messa, and G. Tieghi, *Europhys. Lett.* **53**, 497 (2001).
- ¹⁹J. A. Barker, *Lattice Theories of the Liquid State* (Pergamon, Oxford, 1963).
- ²⁰G. Y. Onoda and E. G. Liniger, *Phys. Rev. Lett.* **64**, 2727 (1990).
- ²¹D. Weaire, J. P. Kermode, and J. Wejchert, *Philos. Mag. B* **53**, L101 (1986).
- ²²H. Hermann, H. Wendrock, and D. Stoyan, *Metallography* **23**, 189 (1989).
- ²³K. Gotoh, *Phys. Rev. E* **47**, 316 (1993).
- ²⁴E. L. Hinrichsen, J. Feder, and T. Jossang, *Phys. Rev. A* **41**, 4199 (1990).
- ²⁵I. Z. Fisher, *Statistical Theory of Liquids* (The University of Chicago Press, Chicago, 1964).
- ²⁶J. Spanier and K. B. Oldham, *An Atlas of Functions* (Hemisphere, WA, 1987).
- ²⁷C. E. Shannon, *Bell Syst. Tech. J.* **27**, 379 (1948), available at <http://cm.bell-labs.com/cm/ms/what/shannonday/paper.html>
- ²⁸E. T. Jaynes, *Phys. Rev.* **106**, 620 (1957).
- ²⁹E. T. Jaynes, in *The Maximum Entropy Formalism*, edited by R. D. Levine and M. Tribus (MIT, Cambridge, MA, 1979), available at <http://bayes.wustl.edu/>
- ³⁰R. Englman, N. Rivier, and Z. Jaeger, *Philos. Mag. B* **56**, 751 (1987).
- ³¹E. T. Jaynes, *Am. J. Phys.* **33**, 391 (1965).
- ³²I. S. Gradshteyn and I. M. Ryzhik, *Table of Integrals, Series and Products*, 6th ed. (Academic, San Diego, New York, 2000).
- ³³See EPAPS Document No. E-JCPSA6-123-509531 for an error analysis of the 2Γ and 3Γ models for hard-disk and hard-sphere structures. This document can be reached via a direct link in the online article's HTML reference section or via the EPAPS homepage (<http://www.aip.org/pubservs/epaps.html>).
- ³⁴W. W. Wood, *J. Chem. Phys.* **48**, 415 (1967).
- ³⁵L. V. Woodcock, *J. Chem. Soc., Faraday Trans. 2* **72**, 1667 (1976).
- ³⁶M. A. Glaser and N. A. Clark, *Adv. Chem. Phys.* **83**, 543 (1993).
- ³⁷V. S. Kumar and V. Kumaran, *J. Chem. Phys.* **123**, 074502 (2005).
- ³⁸J. G. Kirkwood, *J. Chem. Phys.* **18**, 380 (1950).
- ³⁹M. H. Cohen and G. S. Grest, *Phys. Rev. B* **20**, 1077 (1979).
- ⁴⁰G. S. Grest and M. H. Cohen, *Adv. Chem. Phys.* **48**, 455 (1981).
- ⁴¹M. H. Cohen and G. S. Grest, *Phys. Rev. B* **26**, 6313 (1982).
- ⁴²T. L. Hill, *Statistical Mechanics* (McGraw-Hill, New York, 1956).
- ⁴³W. G. Hoover, *J. Chem. Phys.* **44**, 221 (1966).
- ⁴⁴H. G. Hanson, *J. Stat. Phys.* **30**, 591 (1983).
- ⁴⁵L. Tonks, *Phys. Rev.* **50**, 955 (1936).
- ⁴⁶J. M. H. Levelt and E. G. D. Cohen, in *Studies in Statistical Mechanics*, edited by J. D. Boer and G. E. Uhlenbeck (North-Holland, Amsterdam, 1964), Vol. II, Pt. B.
- ⁴⁷I. C. Sanchez, *J. Chem. Phys.* **101**, 7003 (1994).
- ⁴⁸B. J. Alder and T. E. Wainwright, *Phys. Rev.* **127**, 359 (1962).
- ⁴⁹W. G. Hoover and F. H. Ree, *J. Chem. Phys.* **49**, 3609 (1968).
- ⁵⁰J. G. Berryman, *Phys. Rev. A* **27**, 1053 (1983).
- ⁵¹M. Tanemura, VISUAL MATH 3, 2001, available at <http://www.mi.sanu.ac.yu/vismath/proceedings/tanemura.htm>
- ⁵²T. Kiang, *Z. Astrophys.* **64**, 433 (1966).
- ⁵³S. B. DiCenzo and G. K. Wertheim, *Phys. Rev. B* **39**, 6792 (1989).
- ⁵⁴A. L. Hinde and R. E. Miles, *J. Stat. Comput. Simul.* **10**, 205 (1980).
- ⁵⁵P. N. Andrade and M. A. Fortes, *Philos. Mag. B* **58**, 671 (1988).
- ⁵⁶E. J. J. van Rensburg, *J. Phys. A* **26**, 4805 (1993).
- ⁵⁷M. J. Maeso and J. R. Solana, *J. Chem. Phys.* **99**, 548 (1993).
- ⁵⁸D. A. Young and B. J. Alder, *J. Chem. Phys.* **70**, 473 (1979).
- ⁵⁹N. F. Carnahan and K. E. Starling, *J. Chem. Phys.* **53**, 600 (1970).
- ⁶⁰W. W. Wood, *J. Chem. Phys.* **20**, 1334 (1952).